ACS APPLIED MATERIALS & INTERFACES

Research Article

www.acsami.org

Novel CO_2-Capture Derived from the Basic Ionic Liquids Orientated on Mesoporous Materials

Mi Mi Wan,[†] Hao Yue Zhu,[‡] Yan Yan Li,[†] Jing Ma,[§] Shuai Liu,[§] and Jian Hua Zhu*,[†]

[†]Key Laboratory of Mesoscopic Chemistry of MOE, College of Chemistry and Chemical Engineering, Nanjing University, Nanjing 210093, China

[‡]Department of Chemistry, The Pennsylvania State University, University Park, Pennsylvania 16802, United States

[§]Kuang Yaming Honored School, Nanjing University, Nanjing 210093, China

Supporting Information

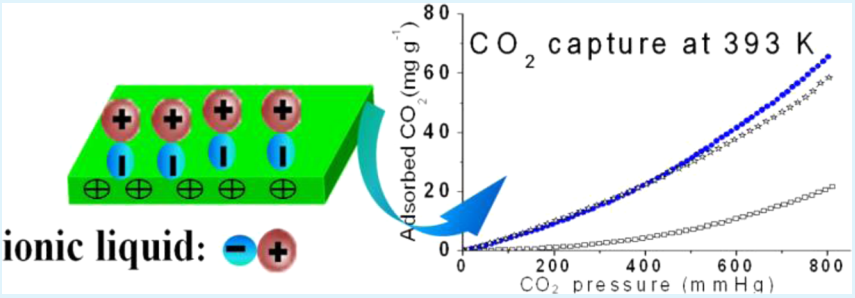

ABSTRACT: Two new basic ionic liquids (ILs) are designed and synthesized in order to conquer the challenge arising from the capture of CO_2 in flue gas whose temperature is over 373 K, and they possess a suitable basic strength to adsorb CO_2 at 393 K with the capacity of 22−49 mg g^{-1}. After these ILs are immobilized on mesoporous alumina or silica, equimolar CO_2 capture is realized at 393 K for the first time. Besides, these adsorbents can be regenerated at 443 K to form a feasible cycle for controlling CO_2 emission in flue gas. Theoretical calculations indicated the key role played by the mesoporous support in promoting CO_2 adsorption via electrostatic interactions between support and ILs. An unwonted promotion of the support's ζ-potential on the performance of ILs is revealed, which induces the immobilized ILs to be oriented in a favorable dispersion, enhancing the efficiency of ILs in the CO_2 adsorption at elevated temperature. This study proposes a new strategy for the sustainable development of novel adsorbent.

KEYWORDS: *basic ionic liquid, CO_2 capture at high temperature, environment protection, flue gas, mesoporous alumina*

1. INTRODUCTION

Fossil fuels provide ca. 87% of the world's energy,[1] but the released CO_2 from coal-fired plants accounts for about 33−40% of global CO_2 emissions.[2] Capturing and sequestering CO_2 in exhaust streams of fossil combustion is thus crucial but challenging because of the relative high temperature of flue gas up to 403−473 K.[3] Even though it is quite possible to cool the flue gas below 373 K and then conventional zeolites can be used, this process will need much more power input and greatly decreases the generating efficiency.[2] There are many other materials used to adsorb CO_2 at lower temperature, such as functionalized SBA-15 silica,[3b] alkali metal exchanged ferrierites,[3c] and sulfur-doped carbons, which shows high adsorption capacities of CO_2 at 273 K (4 mmol g^{-1}).[3d] However, zeolites, activated carbon, hydrotalcite, and most of the metal organic framework (MOF) are weak to trap CO_2 once the temperature exceeds 373 K, and the application of alkali metal oxide or alkali earth metal oxides is limited by their high regeneration temperature up to 1173 K,[4−6] while amine-based sorbents suffer from the drawback of evaporative loss and degradation.[7−10] Thus, fabricating new basic sorbent permitting efficient CO_2 capture in flue gas with mild regeneration temperature in the range 373−473 K is a great challenge spurring the development of new functional materials. Ionic liquids (ILs) are competitive candidates due to their negligible vapor pressures, high thermal stability, and tunable properties.[11] They preserve the proper basicity similar to that of amines and have a higher thermal stability. Particularly, many excellent properties of ILs such as high capacity, low absorption enthalpy, and outstanding reversibility can be achieved by tuning their structure.[12−14] For instance, Wang et al.[13] designed the basic ILs, [P66614] [Im] (trihexyl(tetradecyl)phosphonium imidazole) to achieve equimolar CO_2 capture at 293 K. However, CO_2 adsorption by ILs has been confined so far to ambient temperature, similar as that by amines (below 373 K). Besides, the absolute absorption amount of CO_2 by [P66614] [Im] at 293 K was about 80 mg g^{-1} owing to its large molar mass (almost 550 g mol^{-1}), and this value is far less than that by

Received: May 10, 2014
Accepted: July 17, 2014
Published: July 17, 2014

amine-supported sobents (237 mg g^{-1} at 308 K).[15] Thus, design and synthesis of new basic ILs with a smaller molar mass for the CO_2 adsorption at relatively high temperature are imperative. Here, P4444 (tetrabutylphosphonium) is chosen as cation for the new IL because of its thermal stability and small molar mass. It contains short alkyl chains so the new IL will have a free volume smaller than that with long alkyl chains (P66614), which enables more ILs to be accommodated into the support with a fixed pore volume to elevate the adsorption efficiency of CO_2. Two anions are selected; imidazole with a good basicity will be combined with P4444 to form the IL named as PI while 3-aminopyrazole is used to produce the IL denoted as PAP that owns more CO_2 adsorption sites (Scheme 1).

Scheme 1. Optimized Structure of Ionic Liquids PAP (left, Mw = 341) and PI (right, Mw = 326)

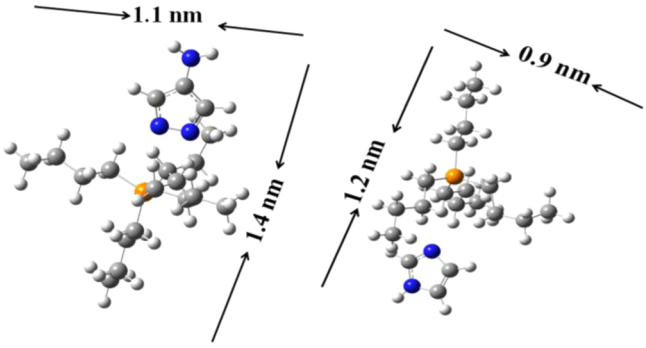

It is generally accepted that immobilization of ILs onto porous supports is promising for CO_2 removal,[16] enhancing the mass transfer rate of CO_2 in sorbent and exerting the efficiency of ILs themselves. The interactions between support and guest such as relative weaker noncovalent or multipoint van der Waals interactions can result in the quite strong binding of the guests with the support cavities, bringing out remarkable changes in the physicochemical properties of guest molecules.[17] Recently, the surface electrostatic property of support, usually characterized by ζ-potential, is also reported to have a big impact on the dispersion of enzyme[18] and release of drugs,[19] but its influence on the immobilization of IL is unknown. Several porous materials are thus selected here as the supports for IL to fabricate the new efficient adsorbent trapping CO_2 at elevated temperature. Among them, mesoporous alumina will be emphatically investigated because of its success in fabrication of efficient CO_2 adsorbent and new superbasic material.[5,20] The special surface state of alumina enabled MgO microcrystalline to insert into framework forming the concert-like structure and adsorbing CO_2 in 423−673 K,[5] while KNO_3 guest was decomposed to form the superbasic species of K_2O.[20] Unlike mesoporous silica keeping a negative ζ-potential,[18,19] the ζ-potential of porous alumina is capable to be adjusted by varying its synthesis conditions and pore structure,[21] which is expected to have a positive effect on the immobilization and CO_2 adsorption of ILs.

To the best of our knowledge, no ILs have been reported to capture CO_2 at the temperature above 373 K. For this challenge, the property function of new ILs and their immobilization on porous support will be carefully studied in order to fabricate the new sorbent capturing CO_2 above 373 K but being regenerated below 493 K, since saving regeneration energy is also crucial for the whole process of capturing and sequestering CO_2. Going forward, three types of porous materials, silica, alumina, and carbon, are employed to evaluate the influence of support on the loading and function of ILs, while two ILs, with or without amino group, are assessed to study the role played by amino group that is the main force of amine-based sorbent. These immobilized ILs will be assessed in the instantaneous CO_2 adsorption at very harsh condition[6] to examine their actual performance. Especially, the possible deactivation of CO_2 sorbent caused by amino group that occurred in amine-based CO_2 sorbents[5,9] will be investigated to seek countermeasure.

2. EXPERIMENTAL SECTION

Materials. Tetrabutylphosphonium bromide ([P4444] Br), 3-aminopyrazole, and imidazole (J&K chemical, China) were analytical grade. The anion-exchange resin (Dowex Monosphere 550A (OH)) was obtained from Dow Chemical Company. Activated carbon (abbreviated as AC) made from coconut shell with a surface area of about 1300 m^2 g^{-1} and the most probable pore size of 1 nm was provided by British American Tobacco.[23] Graphene oxide (GO) with a surface area of 327 m^2 g^{-1} was synthesized consulting literature.[24] Zeolite NaY was purchased from market. All chemicals were obtained in the highest purity grade available and used as received.

Synthesis of Basic ILs. A solution of [P4444] OH in water was prepared from [P4444]Br using an anion-exchange resin. Afterward, the [P4444][OH] solution was neutralized with equimolar quantities of 3-aminopyrazole or imidazole, and the mixture was evaporated under reduced pressure at 353 K and then dried with P_2O_5 under vacuum at 353 K for 48 h. The obtained ILs was denoted as PAP or PI.

Synthesis of SBA-15 (abbreviated as S15), MCM-41 (M41), MCM-48 (M48), and p-alumina (pA, which means mesoporous alumina) were prepared according to refs 4, 25−28. The IL modified absorbents were prepared by impregnation method as in the literature.[29] A given amount of ILs was dissolved in 10 g of ethanol under stirring for 0.5 h, and then, 0.2 g of the support was added into the solution. After stirring and refluxing for 2 h, the mixture was evaporated at 353 K, followed by drying at 373 K for 1 h. These composites are denoted as *n*IL/support, where *n* represents the weight percentage of ILs in the sample, and the support is M41, M48, S15, pA, GO, or AC.

Characterizations. X-ray diffraction (XRD) patterns of samples were recorded on an ARL XTRA diffractometer (power 40 kV, 40 mA) using Cu Kα radiation in the 2-θ range 6−90° or 0.6−6°. N_2 adsorption−desorption isotherms were measured on a Micromeritics ASAP 2020 system at 77 K, and the sample was evacuated at certain temperature for 4 h prior to test. The Brunauer−Emmett−Teller (BET) method was utilized to calculate the specific surface areas of samples using adsorption branches acquired at the relative pressure (P/P_0) range 0.05−0.22, and the total pore volume was estimated from the amount adsorbed at a relative pressure (P/P_0) of 0.99. Pore size distribution curves were calculated by using the improved Kruk−Jaroniec−Sayari (KJS) method,[27b] and the primary mesopore size of samples was estimated on the basis of the relative pressure of the condensation step in the adsorption branches of the isotherms. The morphology of the sample was observed by scanning electron microscopy (SEM) using a Hitachi S4800 FE-SEM system with 10 kV accelerating voltage and 10 mA of beam current, while transmission electron microscopy (TEM) analysis was carried out on a JEM-1011 electron microscope operating at 200 kV. The Fourier transform infrared (FT-IR) spectra were recorded on a NEXUS870 spectrometer, and the sample was mixed with KBr.[6] The experiment of ^1H NMR was performed on a set of Bruker DPX-500 spectrometer, in which DMSO was used as solvent. Thermogravimetric analysis (TGA) of the IL-based adsorbent was performed on a STA 449 C instrument under N_2 atmosphere with a heating rate of 10 K min^{-1}.

To assess the instantaneous adsorption ability of the sample under dynamic conditions,[6] 30 mg of the sample was activated at a given temperature such as 393 K for 1 h, and then, 0.164 mL of CO_2 was

Table 1. Physicochemical Properties of the Samples

samples	S_{BET} ($m^2 \cdot g^{-1}$)	V_p ($cm^3 \cdot g^{-1}$)	D_{BJH} (nm)	ζ-potential (mV)	amount of IL (mmol g^{-1}, A)	CO_2 ads. (mmol g^{-1}, B)	B/A
MCM-41	1118	0.94	2.4	−20.0	0	0.10	
15PAP/M41	308	0.23	2.4	−57.7	0.44	0.21	0.48
33PAP/M41	32	0.03		−60.1	0.97	0.51	0.53
50PAP/M41	7.5	0.01		−65.4	1.47	1.45	0.97
67PAP/M41	5.7	0.005		−66.5	1.96	1.84	0.94
15PI/M41	821	0.61	2.6	−59.3	0.46	0.17	0.37
33PI/M41	245	0.15	2.2	−62.7	1.01	0.19	0.19
50PI/M41	18	0.04		−65.7	1.53	0.64	0.42
67PI/M41	2	0.002		−68.4	2.05	0.91	0.44
p-Al_2O_3	322	0.74	4.3	51.1	0	0.23	
15PAP/pA	277	0.31	4.3	39.0	0.44	0.49	1.11
33PAP/pA	36	0.19		39.1	0.97	0.80	0.82
50PAP/pA	13	0.035		3.8	1.47	1.20	0.79
15PI/pA	241	0.26	4.2	45.0	0.46	0.65	1.41
33PI/pA	42	0.23		32.1	1.01	1.02	1.0
50PI/pA	6.5	0.03		−9.3	1.53	1.16	0.76

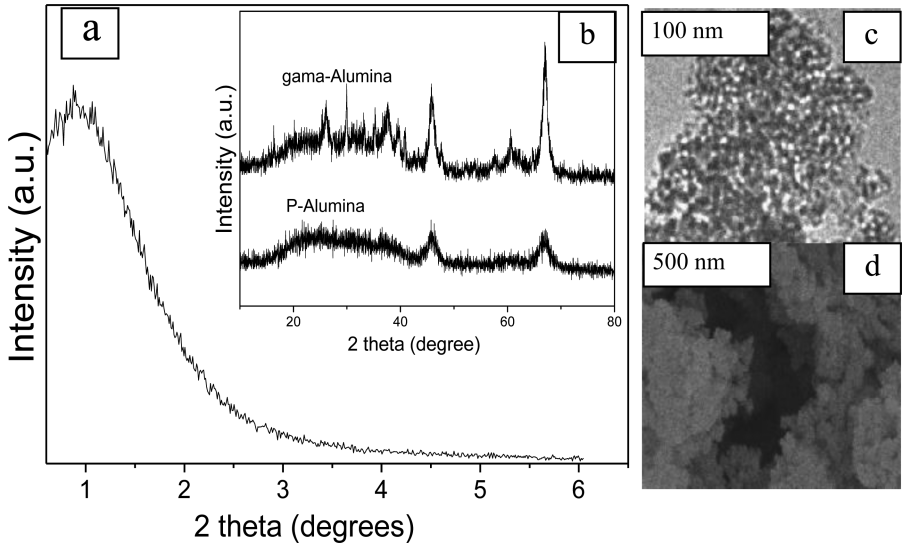

Figure 1. Low-angle (a) and wide-angle (b) XRD patterns, TEM (c) and SEM images of p-alumina (pA) sample.

injected each time accompanied by carrier gas (30 mL min^{-1}). The residual CO_2 was detected by an "online" Varian 3380 gas chromatograph and quantitatively measured by the external standard method.[6] Adsorption amount of CO_2 by the samples for 15 injections was denoted as mg CO_2 per gram of sorbent. To test the cycling ability of sample, it was assessed in dynamic CO_2 adsorption at 393 K as mentioned above. After then, the adsorbent was regenerated at 443 K for 30 min under nitrogen atmosphere, and then, it was cooled again to 393 K to start another cycle of CO_2 adsorption. Mass signals were recorded on Ametek Dycor LC-D200 instrument during the desorption process. On the other hand, the CO_2 adsorption isotherms of ILs-based sample were measured using a Micromeritics ASAP 2020 static volumetric analyzer at the setting temperature.[6] Prior to adsorption experiment, the sample was degassed at 393 K for 12 h, followed by introduction of CO_2 into the system. The gas adsorption amount was then recorded in terms of adsorbed volume under standard temperature and pressure (STP). With the assistance of the equation $PV = nRT$, these data were converted to the amount of CO_2 (mmol g^{-1}) at ordinary pressure (1 atm).

In situ FT-IR spectra of CO_2 adsorbed on the immobilized ILs were recorded on a Nicolet 5700 FT-IR spectrometer. The sample was purged with N_2 for 60 min at certain temperatures prior to taking a background spectrum, and then exposed to a stream of CO_2 at a rate of 10 mL min^{-1} for 10 min, followed by a purge with N_2 for 60 min. Finally, the sample was heated to 473 K to release the adsorbed CO_2. All spectra were taken at certain temperature and the corresponding background subtracted from them.

All calculations were performed by using the Gaussian03 programs package.[28] For each set of calculation, we calculated geometry and energy optimizations for each IL, the free CO_2 molecule, and each ILs−CO_2 complex at the B3LYP/6-31g level.

3. RESULTS

3.1. Preparation and Immobilization of Basic Ionic Liquids. The structure of new-designed basic ILs (Scheme 1) is verified by FT-IR and ^1H NMR measurements. As shown in Supporting Information Figure S1, reactant P had a band of $-CH_3$ at about 2900 cm^{-1}, and reactant AP was characterized with the band of $-NH_2$ near 1600 cm^{-1};[22] these two bands were observed on the spectrum of ionic liquid PAP, demonstrating the successful combination of positive and negative parts. Also, the spectrum of PI possessed the band of $-CH_3$ at around 2900 cm^{-1} and the character of 1052 cm^{-1} that is the C−H bond in-plane bending vibrations in imidazole ring[30] originating from reactant I. Besides, ^1H NMR data of PAP were (Supporting Information Figure S1): 0.93 (m, 12 H, CH_3), 1.39−1.46 (m, 16H, $(CH_2)_2$), 2.12−2.25 (m, 8H, P-

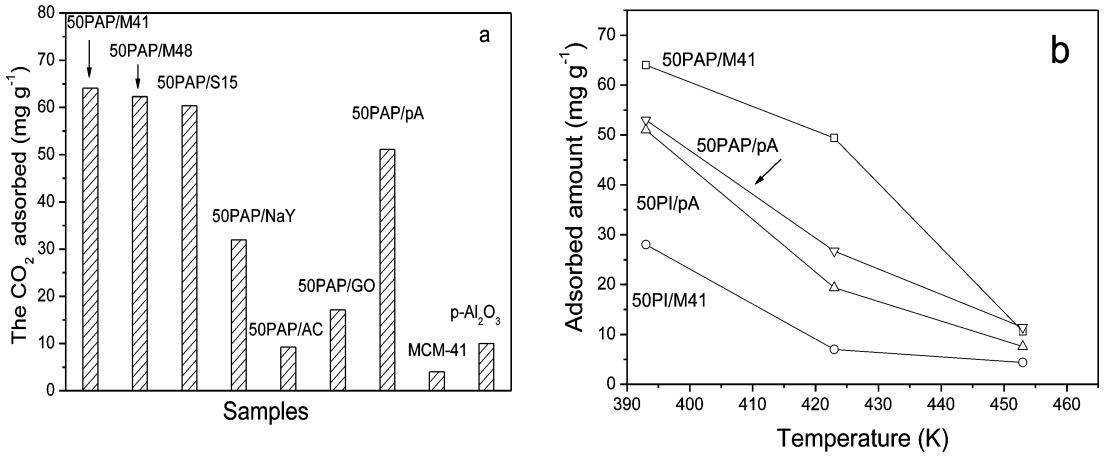

Figure 2. Instantaneous adsorption of CO_2 on various porous materials (a) loaded with PAP at 393 K and (b) at different temperatures.

CH_2), 6.95 (s, 2H, C_4 and C_5), 3.6 (s, 1H, NH_2), and the data of PI were: 0.92 (m, 12 H, CH_3), 1.38−1.49 (m, 16H, $(CH_2)_2$), 2.14−2.22 (m, 8H, P-CH_2), 6.8 (s, 2H, C_4 and C_5).

Several porous materials were selected to support these basic ILs, including mesoporous alumina (pA), mesoporous silica such as MCM-41 (abbreviated as M41), MCM-48 (M48), SBA-15 (S15), and zeolite NaY, graphene oxide (GO) as well as activated carbon (AC), and their textual properties are listed in Table 1 and Supporting Information Table S1. Besides, their N_2 adsorption−desorption isotherms are shown in Supporting Information Figure S3. Low-angle XRD pattern of pA sample (Figure 1a) illustrates a single broad reflection with 2-θ value of 1°, which is a character of the mesoporous structure without long-range order in the pore arrangement.[31] Some very diffuse and weak reflections were observed in the wide-angle XRD patterns of pA sample (Figure 1b), representing a crystalline phase similar to that of γ-Al_2O_3. According to the images of TEM and SEM (Figure 1c and d), pA sample had the worm-like pore structure and big agglomerated particles of several micrometers with rough surface. Besides, pA has a positive ζ-potential (51.1 mV, Table 1), opposite to that of M41 (−20 mV).

After immobilization of ILs, all mesoporous supports kept their structure (Supporting Information Figure S4a, b, and c), let alone those microporous materials such as zeolite and activated carbon. As the amount of ILs rose to 50 wt %, the XRD peak of 50PAP/pA sample became indistinct (Supporting Information Figure S4c); meanwhile, 67PAP/M41 retained its mesoporous structure, which might result from their different surface areas (Table 1). Therefore, pA and M41 were chosen to be emphatically studied in succeeding research. In the case of M41 or pA with immobilized IL no more than 33 wt %, they exhibited a kind of type IV isotherm with big uptake at high partial pressures in N_2 adsorption−desorption test (Supporting Information Figure S5a and c); however, this character was lost when the loading amount reached 50 wt %. Also, the pore size distribution of these immobilized samples was changed. Especially, loading 33 wt % of PAP or PI filled the small pores of about 4 nm in pA, and the loading amount of 50 wt % blocked the pores of around 30 nm (Supporting Information Figure S5d), since the organic liquid preferably fills the small pores of support due to the optimal surface tension and host−guest interaction.

A strange influence of dispersing IL on the surface area of porous supports was observed on pA and M41. Immobilization of PAP on M41 made the surface area of 15PAP/M41 lowered from 1118 to 308 $m^2\ g^{-1}$ (Table 1). Apart from the part caused by the reduced proportion of M41 (85%) in sample (theoretically, 168 $m^2\ g^{-1}$ Supporting Information Table S2), loading the guest PAP consumed a surface area of about 642 $m^2\ g^{-1}$. In contrast, dispersing 15 wt % of PI on M41 reduced the value from 1118 to 821 $m^2\ g^{-1}$, and the part caused by loading IL was 129 $m^2\ g^{-1}$. As the amount of IL guest rose to 33 wt %, this difference was decreased; 717 $m^2\ g^{-1}$ was reduced by loading PAP while 504 $m^2\ g^{-1}$ by PI on M41 support. Nonetheless, it is very strange that the surface area of 15PAP/pA sample (277 $m^2\ g^{-1}$) was 14% smaller than that of pA (322 $m^2\ g^{-1}$) as if no surface area was consumed by the loading guest, while 33 $m^2\ g^{-1}$ of reduced surface area was found on 15PI/pA composite, much smaller than that of 15PI/M41 (129 $m^2\ g^{-1}$). Similarly, the values of 180 and 174 $m^2\ g^{-1}$ were calculated on the samples of 33PAP/pA and 33PI/pA, respectively, also less than those of 33PAP/M41 and 33PI/M41. The mesoporous sorbents containing template and/or amine inside channels usually showed a very small surface area in N_2 adsorption measurement,[15,29,32] since nitrogen diffusion barrier in the organic bulk could hardly be overcome at low temperature, but the reason why mesoporous alumina with a relative small surface area kept a relative higher ratio of residual value is unknown.

The immobilized ILs kept a better thermal stability than the free ILs did (Supporting Information Figure S6), and their decomposition temperature on the composite of 50PAP/M41, 50PI/M41, 50PAP/pA, and 50PI/pA was 450 K, 473 K, 460 K, and 500 K, respectively, higher than that of PAP (420 K) and PI (430 K). To further check the thermal stability of ILs supported on M41, two other samples, 67PAP/M41 and 33PI/M41, were purged at 473 K in a N_2 flow for 2 h prior to FT-IR test. No obvious change was observed on the spectra of 33PI/M41 (Supporting Information Figure S7a), but the band of amino group at about 1600 cm^{-1} disappeared on that of 67PAP/M41 treated at 473 K (Supporting Information Figure S7b). However, this amino group of 67PAP/M41 was stable at 463 K at least 2 h, which guarantees the application of immobilized ILs at 453 K.

3.2. Adsorption of CO_2 at 393 K by Immobilized ILs.

Immobilization of ILs on mesoporous supports such as MCM-41, MCM-48, SBA-15, and pA significantly enhances the CO_2 adsorption capability of IL at 393 K (Figure 2a), even in the harsh instantaneous adsorption test in which the contact time

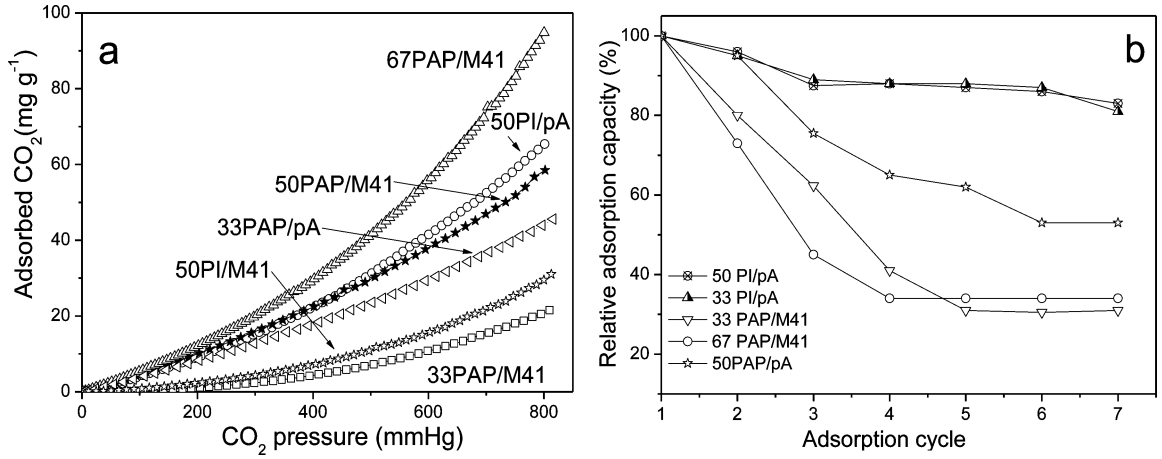

Figure 3. CO_2 adsorption isotherms at 393 K (a) and the recycle instantaneous CO_2 adsorption of supported ionic liquids (b).

with CO_2 is shorter than 2 s and the CO_2 concentration in gas flow is about 5%.[6] With 50 wt % of PAP dispersed, these adsorbents exhibited a capacity of 51−64 mg g^{-1} at 393 K, which was even higher than that of PAP itself (49 mg g^{-1}). However, zeolite NaY, graphene oxide (GO), and activated carbon (AC) failed to promote the CO_2 adsorption capability of PAP, and the capacities of PAP immobilized on these materials were no more than 30 mg g^{-1} (Figure 2a). To investigate how the surface roughness of support affects the immobilization of ILs, small amount of PAP (15%) was loaded on SBA-15 and MCM-41 and its CO_2 adsorption capacity at 393 K was assessed. According to the study of Zukal et al.,[31b] grafting of substance on SBA-15 leads to the plugging of micropores and thus the smoothing of mesopore surface will first take place. Therefore, 15% of IL will first plug the micropores of SBA-15, which will prevent some adsorption sites from capturing CO_2 to some extent. As a result, CO_2 adsorption capacities of 15PAP/S15 and 15PAP/M41 were 5.3 and 9.1 mg/g, respectively. Both surface roughness and the negative charged surface property can induce the deactivation of IL when the immobilized amount is low. That is why 15PAP/S15 exhibits a lower adsorption capacity than that of 15PAP/M41. As the amount of PAP loaded on M41 rose from 15 wt % to 67 wt %, the composite captured more and more CO_2 increased from 9.2 to about 81 mg g^{-1} (0.21 to 1.84 mmol g^{-1}) despite of its surface area became smaller and smaller (Table 1). The same tendency was also found on *n*PI/M41 series samples, whose capacity rose from 0.17 to 0.91 mmol g^{-1}, which was smaller than that of corresponding *n*PAP/M41 composite though the surface area of 15PI/M41 and 33PI/M41 was larger than that of 15PAP/M41 and 33PAP/M41 (Table 1). This difference means the important role played by the amino group of IL in the sorbent for CO_2 adsorption. An unwonted phenomenon is observed on pA support whose surface area is much smaller than that of M41. The same amount of PAP or PI immobilized on pA could capture more CO_2 than that on M41 except 50PAP/pA sample (Supporting Information Figure S8a). Especially 15PAP/pA adsorbed 130% more CO_2 than 15PAP/M41, while 15PI/pA trapped 280% more than 15PI/M41 though its surface area was 70% smaller. For the first time, equimolar adsorption of CO_2 by IL at 393 K was realized on the sample of 15PAP/pA, 15PI/pA, 50PAP/M41, and 67PAP/M41 where the molar ratio of CO_2/IL reached to 1.11, 1.47, 0.97, and 0.94, respectively (Table 1). As expected, the temperature of adsorption strongly affects the performance of PAP-based composites (Figure 2b), 50PAP/M41 sorbent captured more CO_2 at 393 K (64 mg g^{-1}) than those at 423 K (49 mg g^{-1}) and 453 K (10 mg g^{-1}), while 50PI/M41 and 50PI/pA samples trapped 6 times more CO_2 at 393 K than that at 453 K, which is beneficial to establish a feasible CO_2 adsorption−desorption cycle in the range 393−453 K, conquering the inherent drawback of amine-dispersed CO_2 sorbents.

To check the CO_2 adsorption results obtained in the instantaneous adsorption, some IL immobilized composites were evaluated in the static CO_2 adsorption at 393 K. As demonstrated in Figure 3a, 67PAP/M41 sample captured about 84 mg g^{-1} of CO_2 (1.91 mmol g^{-1}), equaling the CO_2/IL molar ratio of 0.97 and thus reappearing the equimolar CO_2 adsorption by IL at 393 K. Also, many trends found in the static adsorption were similar to that observed in the instantaneous adsorption, for instance, the high IL content of sorbent was beneficial for the CO_2 adsorption in the static condition, and the PAP guest was more active on the support of M41 than PI did, while the same amount of PAP or PI immobilized on pA carrier could adsorb more CO_2 than that on M41. The similar capability of most sorbents exhibited in both static and dynamic CO_2 adsorptions confirms the consistency of the results obtained in two methods.[6] Figure 3b showed the CO_2 adsorption−desorption recycling performance of IL immobilized sorbents, since the stability of adsorbent is important for its potential application. Mesoporous alumina pA had a special function in the seven cycles of adsorption (393 K)−desorption (443 K), in which the relative adsorption capacities of 50PI/pA and 33PI/pA samples tardily declined from 100% to 96% then 87% and finally to 81−83%. When the PI guest was replaced by PAP, the resulting 50PAP/pA sample exhibited an obvious declined capacity and the final value was 53%. More serious recession appeared on the composites of 67PAP/M41, whose adsorption capacity fleetly lost more than 60% in the fourth cycles, and same trend was found on its analogue 33PAP/M41, validating the deactivation. Nonetheless, these recycled sorbents kept the structural characters of their support as demonstrated by the XRD measurement (Supporting Information Figure S 4d); that is to say, the deactivation is caused by the variation of the IL guests on their supports. Moreover, only the mass spectrum signal of CO_2 was detected from 67PAP/M41 sorbent during the desorption process (Supporting Information Figure S8b), excluding the suspicion whether IL was lost from the adsorbent in the regeneration. It

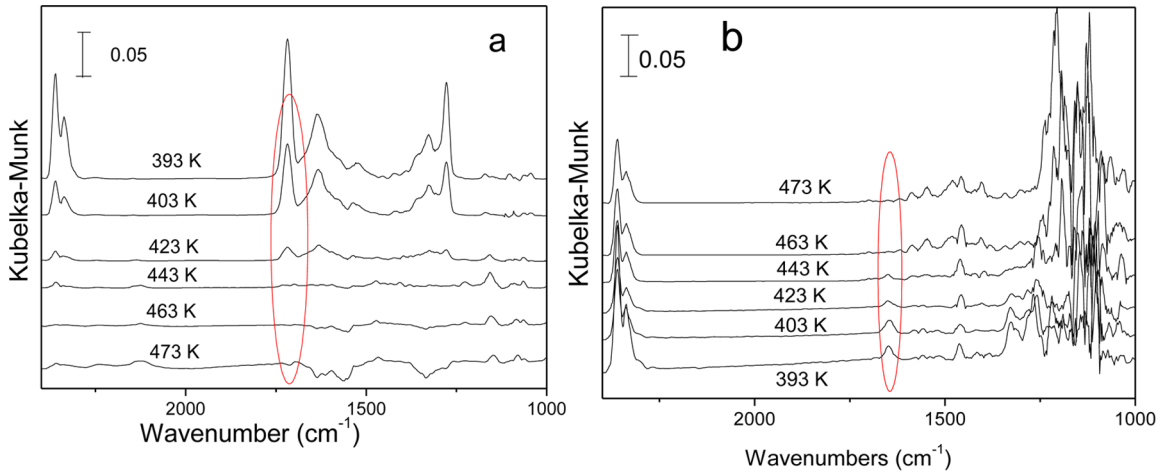

Figure 4. In situ FT-IR spectra of the CO_2 on (a) 50 PI/pA and (b) 67PAP/M41 samples at different temperatures.

should point out that, apart from its higher initial adsorption ability (81 mg g^{-1}), 67PAP/M41 was able to show the absolute capacity (about 30 mg g^{-1}) close to that of 50PI/pA (~40 mg g^{-1}) in the cycle tests.

The adsorption of CO_2 on the IL-immobilized composites was also investigated by in situ FT-IR method (Figure 4). In the spectrum of 50PI/pA sample adsorbed CO_2 at 393 K, two bands appeared at around 1700 and 1630 cm^{-1} resulting from C═O stretch,[12,33] while these of about 1280 and 1310 cm^{-1} confirmed the C—O stretching.[34] The bands at 2350 cm^{-1} could be attributed to gas phase CO_2.[35] All of these bands were weakened at elevated temperature and finally disappeared at 463 K (Figure 4a). On the spectrum of 67PAP/M41 adsorbed CO_2 at 393 K, the bands at about 1650 and 1320 cm^{-1} originated from the formation of C═O[22] and C—O groups,[34] resulting from the CO_2 adsorption by negative N^- on pyrazole ring. Both bands declined as the temperature increased from 393 to 443 K and disappeared at 463 K due to desorption of CO_2 (Figure 4b). Meanwhile, the bands at about 1550 cm^{-1} (attributed to C═O), 1460 cm^{-1} (C—N bond in urea),[36] and 1250 cm^{-1} (C—N bond in urea)[37] appeared due to the adsorption of CO_2 by amino group of the pyrazole ring, but they kept unchanged at elevated temperature, because the formed urea could not desorb or decompose in the range of temperature.[22] Based on these results, CO_2 adsorption on the basic ILs is inferred to involve the formation of carbonate[12] and urea,[22] and adsorption mechanisms of PAP and PI are illustrated in Scheme 2. Existence of amino group in IL seems to be the double edged sword, which enables PAP to possess more CO_2 adsorption sites than PI does so that it has a theoretical molar CO_2 adsorption of 1.5 (Scheme 2) but inevitable causes the formation of urea with the adsorbed CO_2 through isocyanate intermediate.[3,7,18]

Scheme 2. Possible CO_2 Adsorption Mechanism by Ionic Liquids: PAP (Above) and PI (Below)

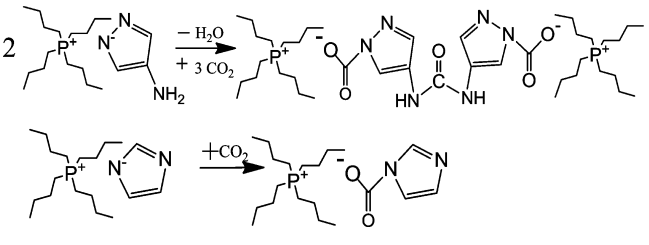

4. DISCUSSION

Two factors, optimized molecular structure and guest−host interaction, endow the new basic ILs to achieve the equimolar adsorption of CO_2 at 393 K. Cation P4444 provides a much smaller MW in comparison with P66614, which is beneficial for the IL to get a higher CO_2 adsorption capacity calculated by per gram of sorbent. Anion of 3-aminopyrazole or imidazole offers the proper basicity, enabling the IL to adsorb CO_2 at 393 K and to be regenerated below 473 K. Immobilization further adjusts the adsorptive performance of ILs. According to the gas-phase reaction energetic calculation at B3LYP/6-31g level of the theory (Supporting Information Table S3), the enthalpy values of CO_2 adsorption for PAP and PI were 22.6 and 12.3 kJ mol^{-1}, respectively. In case they were immobilized on porous silica such asMCM-41, the data changed as 33 and 18 kJ mol^{-1}, and these values were 21 and 31 kJ mol^{-1} when PAP and PI were immobilized on porous alumina such as pA. These variations imply the higher adsorption affinity for CO_2 by immobilized ILs. Enthalpy of CO_2 adsorption is also a commonly parameter used to assess the energy demand for CO_2 adsorption, which is about 80 kJ mol^{-1} for traditional amino-functionalized ILs.[38] As for functionalized SBA-15 silica,[3b] FER zeolites containing Al,[38b] and alkali metal exchanged ferrierites,[3c] the adsorption enthalpies are 10−50, 30−60, and 40−60 kJ mol^{-1}, respectively. From the perspective of energy-saving, designing the proper IL with decreased enthalpy of CO_2 capture is of great significance. A reduction of absolute value of adsorption enthalpy (compared with 80 kJ mol^{-1}) can lead to a decreased energy requirement for regeneration process.

Immobilization of PAP or PI is first governed by the pore size and second by the surface area of support. For example, 50 wt % of PAP could be easily dispersed on mesoporous silica to form the composite like 50PAP/M41, and it was hardly immobilized on pA and graphene oxide whose surface area was below 400 m^2 g^{-1} but very difficult to be loaded on microporous zeolite NaY and activated carbon (AC) though these two porous materials had a surface area larger than 700 m^2 g^{-1} (Supporting Information Table S2). PAP has a molecular size of 1.4 nm × 1.1 nm, so it will be very difficult to enter inside the microporous support. Consequently, PAP immobilized on mesoporous supports displayed a capability

Scheme 3. Schemetic Illustration of the Distribution of the ILs PAP and PI Immobilized on Different Supports MCM-41 and Mesoporous Alumina

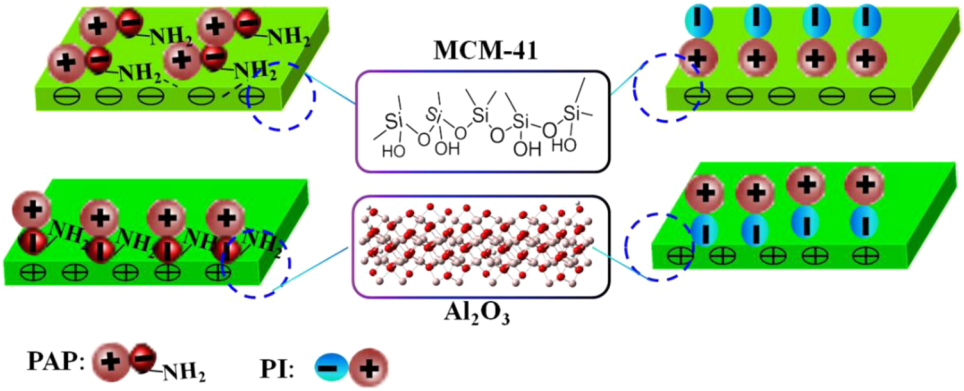

higher than that on microporous ones in the CO_2 capture at 393 K (Figure 2a). According to the size of PAP, 28 wt % of the IL is needed to form a layer on the surface of MCM-41, and 48 wt % is estimated to be fully filled the support, which is in accordance with experiment results. Actually, the surface area of 50PAP/M41 was lowered to less than 10 m^2 g^{-1}, as a result of the full occupation of whole pore space.

The better performance of ILs immobilized on pA than that on M41 when the loading amount was no more than 33% (Table 1), along with the achievement of equimolar CO_2 adsorptions on the samples of 15PAP/pA, 13PI/pA, and 33PI/pA, indicates the unusual promotion of pA support on the guest ILs. This unusual phenomenon may originate from the special dispersion of ILs induced by the essential surface state of support. Mesoporous alumina had a positive ζ-potential of 51 mV, so the anion of the ILs with low loading amount (e.g., 15%) would be attracted while the cation experienced the repulsion from the surface of pA. As a result, PAP would have its anion erected on the surface while cation upturned due to the repulsive force between the support's surface and the cation (Scheme 3); meanwhile, many of the interspaces among these cations were formed enabling N_2 or CO_2 to enter, which could compensate the reduction of surface area or pore volume occupied by PAP guests more or less. This speculation can be verified by the fact that 15PAP/pA kept the positive ζ-potential and a relatively large surface area and pore volume (Table 1) and its actual CO_2 adsorption capacity was higher than that of 15PAP/M41. Likewise, 33PAP/pA composite showed a larger pore volume and CO_2 adsorption capacity than 33PAP/M41. Specific orientation and dispersion of PI molecules might also occur in the sample of 15PI/pA where CO_2 molecule had to go through the upturned cations prior to be adsorbed by the anions in bottom, and these cations functioned as funnels for the adsorbate to direct it into the site, enhancing the sorption process[39] and endowed the 15PI/pA sample to trap 282% more CO_2 than the 15PI/M41 (Table 1) did. As the amount of PI loaded on porous support increased from 15 wt % to 50 wt %, *n*PI/pA composite still captured more CO_2 at 393 K than corresponding *n*PI/M41 (Table 1), demonstrating the unwonted promotion effect. It is this particular orientation of ILs on the surface of pA that enables the adsorbed CO_2 to resist the N_2 purge at 393 K, since the adsorption site in the anion was surrounded tightly by the alkyl chains in cations, keeping the adsorbate within a channel-like microenvironment. What's more, such special arrangement of ILs along with the delicate confinement effect guaranteed the adsorption of CO_2 by the sorbent at higher temperature such as 423 K, conquering the inherent drawback of free IL that failed to hold CO_2 in N_2 stream at about 373 K.[12] Due to the higher affinity of PI/pA with CO_2 than PAP/pA (Supporting Informaion Table S1), the PI immobilized on pA was more active to capture CO_2 than the PAP on the support (Table 1). When PI was immobilized on M41, its cation was attracted by the negative charged surface of support (ζ-potential is −20 mV) and the anion was thus upturned due to the repulsive force. As a result, the adsorbed CO_2 by the anion was exposed in the stream of N_2 flow and easily blown away hence the performance of PI/M41 samples was inferior to that of PI/pA composites (Table 1).

Concerning on the PAP immobilized on M41, its cation was attracted by the negative charged silanol groups of mesoporous silica, while its positive charged amino-group in anion would form hydrogen bond with these Si−OH groups; therefore, the anion was exposed on the surface of composite (Scheme 3) when the amount of immobilized PAP was less than the threshold of monolayer (28 wt %). As the result, the whole PAP molecule was bent to cover the surface of MCM-41, lowering both the surface area and the pore volume of sorbent, and an obviously increased value (−57 mV) was observed on 15PAP/M41 sample for the anion of PAP was exposed as mentioned above (Scheme 3). The ζ-potential value rose to −60.1 mV when the immobilized amount of PAP changed to 33 wt %; then, it achieved −65.4 mV, and further immobilizing more PAP no longer enhanced this value because the support was fully filled. Thus, both 55PAP/M41 and 67PAP/M41 showed similar surface areas (Table 1). Since the amino groups of 15PAP/M41 and 33PAP/M41 were linked with silanol group, hindering the access of CO_2, these sorbents showed low capability in the adsorption of CO_2 (Table 1). The surface Si−OH groups of 50PAP/M41 had been covered by the layer of PAP so that the succeeding PAP could exert the high efficiency of adsorbing CO_2; therefore, it adsorbed 64 mg g^{-1} of CO_2.

FT-IR measurement confirmed the different state of amino group in PAP/M41 and PAP/pA samples. The band of amino group at around 1600 cm^{-1} was absent on the spectrum of 15PAP/M41 and 33PAP/M41, since these amino groups interacted with silanol group as that reported on SBA-15[10] but appeared on that of 50PAP/M41 (Figure 5), due to the existence of PAP exceeded the monolayer threshold. To exclude the suspicion whether the amino group of 15PAP/M41 and 33PAP/M41 is lower than the determination limit, the same tests were performed on samples of 15PAP/pA and 33PAP/pA, where the band of amino group clearly emerged,

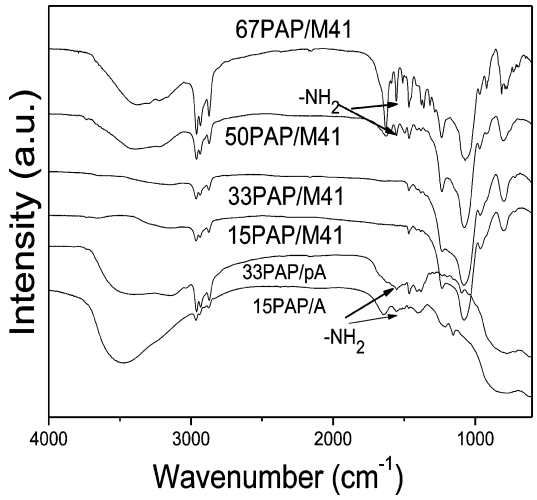

Figure 5. FT-IR spectra of the samples with different amount of ionic liquids.

which verified the interaction between amino group and the silica wall of MCM-41 support. It is conceivable that adjusting the IL-support interactions should prevent the negative interaction of silanol group, and thus, the as-synthesized MCM-41(named as M41-as), whose ζ-potential is +18.7 mV, was chosen as support to confirm this issue, because there was no silanol group on its surface.[15] M41-as itself only trapped 4 mg g^{-1} of CO_2 at 393 K. After being immobilized with 15 wt % PAP, this sample adsorbed 32 mg g^{-1} of CO_2 (0.72 mmol g^{-1}) at 393 K, 246% more than that by 15PAP/M41 and approached the theoretical molar CO_2 adsorption of 1.5, which gives a clue of avoiding such interaction by tailoring the surface property of support. Further investigation is in progress.

5. CONCLUSIONS

In summary, we designed and prepared two new basic ILs for CO_2 capture at the elevated temperature close to that of flue gas. These supported ILs realized the equimolar CO_2 capture at 393 K for the first time, and most of the adsorbed CO_2 could be desorbed at 443 K, forming a feasible adsorption−desorption cycle. Support-induced degradation of MCM-41-supported ILs can be ascribed to its negative charged surface, and selecting the supports with positive charged surface property can effectively avoid this phenomenon. Moreover, an unwonted promotion on the CO_2 adsorption of IL was observed on mesoporous alumina with positive ζ-potential that induced the specific orientation and dispersion of ILs. CO_2 chemisorption system combining ILs PI and mesoporous alumina together could be recycled with minimal loss of activity, opening an avenue for the fabrication of new ILs-based functional materials.

■ ASSOCIATED CONTENT

Supporting Information

Some structural characterizations of the supported ionic liquids and calculated adsorption enthalpy of the samples with CO_2. This material is available free of charge via the Internet at http://pubs.acs.org.

■ AUTHOR INFORMATION

Corresponding Author

*Email: jhzhu@netra.nju.edu.cn.

Notes

The authors declare no competing financial interest.

■ ACKNOWLEDGMENTS

National Science Foundation (NSF) of China (21173117 and 21273106), Graduate School and Analysis Center of Nanjing University financially supported this research. The authors thank Mr. Lin-sen Zhou and Dr. Yong Guo (NJU) for their assistance in molecular calculation.

■ REFERENCES

(1) Tollefson, J.; Monastersky, R. The Global Energy Challenge: A Wash with Carbon. *Nature* **2012**, *491*, 654−655.

(2) Yang, H.; Xu, Z.; Fan, M.; Gupta, R.; Slimane, R. B.; Bland, A. E.; Wright, I. Progress in Carbon Dioxide Separation and Capture: A Review. *J. Environ. Sci. (Beijing, China)* **2008**, *20*, 14−27.

(3) (a) Granite, E. J.; Pennline, H. W. Photochemical Removal of Mercury from Flue Gas. *Ind. Eng. Chem. Res.* **2002**, *41*, 5470−5476. (b) Zukal, A.; Jagiello, J.; Mayerovaa, J.; Cejka, J. Thermodynamics of CO_2 Adsorption on Functionalized SBA-15 Silica. NLDFT Analysis of Surface Energetic Heterogeneity. *Phys. Chem. Chem. Phys.* **2011**, *13*, 15468−15475. (c) Zukal, A.; Pulido, A.; Gil, B.; Nachtigall, P.; Bludsky, O.; Rubes, M.; Cejka, J. Experimental and Theoretical Determination of Adsorption Heats of CO_2 Over Alkali Metal Exchanged Ferrierites with Different Si/Al Ratio. *Phys. Chem. Chem. Phys.* **2010**, *12*, 6413−6422. (d) Seredych, M.; Jagiello, J.; Bandosz, T. J. Complexity of CO_2 Adsorption on Nanoporous Sulfur-Doped Carbons—Is Surface Chemistry an Important Factor? *Carbon* **2014**, *74*, 207−217.

(4) Choi, S.; Drese, J. H.; Jones, C. W. Adsorbent Materials for Carbon Dioxide Capture from Large Anthropogenic Point Sources. *ChemSusChem* **2009**, *2*, 796−854.

(5) Han, K. K.; Zhou, Y.; Chun, Y.; Zhu, J. H. Efficient MgO-Based Mesoporous CO_2 Trapper and Its Performance at High Temperature. *J. Hazard. Mater.* **2012**, *203*, 341−347.

(6) Li, Y. Y.; Han, K. K.; Lin, W. G.; Wan, M. M.; Wang, Y.; Zhu, J. H. Fabrication of a New MgO/C Sorbent for CO_2 Capture at Elevated Temperature. *J. Mater. Chem. A* **2013**, *1*, 12919−12925.

(7) Rochelle, G. T. Amine Scrubbing for CO_2 Capture. *Science* **2009**, *325*, 652−1654.

(8) Liu, A. H.; Ma, R.; Song, C.; Yang, Z. Z.; Yu, A.; Cai, Y.; He, L. N.; Zhao, Y. N.; Yu, B.; Song, Q. W. Equimolar CO_2 Capture by N-Substituted Amino Acid Salts and Subsequent Conversion. *Angew. Chem., Int. Ed.* **2012**, *51*, 11306−11310.

(9) Sayari, A.; Belmabkhout, Y.; Dana, E. CO_2 Deactivation of Supported Amines: Does the Nature of Amine Matter? *Langmuir* **2012**, *28*, 4241−4247.

(10) Wang, X. X.; Schwartz, V.; Clark, J. C.; Ma, X. L.; Overbury, S. H.; Xu, X. C.; Song, C. S. Infrared Study of CO_2 Sorption over "Molecular Basket" Sorbent Consisting of Polyethylenimine-Modified Mesoporous Molecular Sieve. *J. Phys. Chem. C* **2009**, *113*, 7260−7268.

(11) Xing, C.; Guan, J.; Li, Y.; Li, J. Effect of a Room-Temperature Ionic Liquid on the Structure and Properties of Electrospun Poly(Vinylidene Fuoride) Nanofibers. *ACS Appl. Mater. Interfaces* **2014**, *6*, 4447−4457.

(12) Wang, C. M.; Luo, H. M.; Jiang, D. E.; Li, H. R.; Dai, S. Carbon Dioxide Capture by Superbase-Derived Protic Ionic Liquids. *Angew. Chem., Int. Ed.* **2010**, *49*, 5978−5981.

(13) Wang, C. M.; Luo, X. Y.; Luo, H. M.; Jiang, D. E.; Li, H. R.; Dai, S. Tuning the Basicity of Ionic Liquids for Equimolar CO_2 Capture. *Angew. Chem., Int. Ed.* **2011**, *50*, 4918−4922.

(14) Zhang, Y. Q.; Zhang, S. J.; Lu, X. M.; Zhou, Q.; Fan, W.; Zhang, X. P. Dual Amino-Functionalized Phosphonium Ionic Liquids for CO_2 Capture. *Chem.—Eur. J.* **2009**, *15*, 3003−3011.

(15) Yue, M. B.; Sun, L. B.; Cao, Y.; Wang, Y.; Wang, Z. J.; Zhu, J. H. Efficient CO_2 Capturer Derived from As-Synthesized MCM-41 Modified with Amine. *Chem.—Eur. J.* **2008**, *14*, 3442−3451.

(16) Zhang, J. M.; Zhang, S. J.; Dong, K.; Zhang, Y. Q.; Shen, Y. Q.; Lv, X. M. Supported Absorption of CO_2 by Tetrabutylphosphonium Amino Acid Ionic Liquids. *Chem.—Eur. J.* **2006**, *12*, 4021−4026.
(17) Shaikh, M.; Swamy, Y. M.; Pal, H. Supramolecular Host−Guest Interaction of Acridine Dye with Cyclodextrin Macrocycles: Photophysical, pK_a Shift, and Quenching Study. *J. Photochem. Photobiol., A* **2013**, *258*, 41−50.
(18) Wan, M. M.; Lin, W. G.; Gao, L.; Gu, H. C.; Zhu, J. H. Promoting Immobilization and Catalytic activity of Horseradish Peroxidase on Mesoporous Silica Through Template Micelles. *J. Colloid Interface Sci.* **2012**, *377*, 497−503.
(19) Wan, M. M.; Yang, J. Y.; Qiu, Y.; Zhou, Y.; Guan, C. X.; Hou, Q.; Lin, W. G.; Zhu, J. H. Sustained Release of Heparin on Enlarged-pore and Functionalized MCM-41. *ACS Appl. Mater. Interfaces* **2012**, *4*, 4113−4122.
(20) Sun, L. B.; Yang, J.; Kou, J. H.; Gu, F. N.; Chun, Y.; Wang, Y.; Zhu, J. H.; Zou, Z. G. One-Pot Synthesis of Potassium-Functionalized Mesoporous γ-Alumina: A Solid Superbase. *Angew. Chem., Int. Ed.* **2008**, *47*, 3418−3421.
(21) Pedimonte, B. J.; Moest, T.; Luxbacher, T.; von Wilmowsky, C.; Fey, T.; Schlegel, K. A.; Greil, P. Morphological ζ-Potential Variation of Nanoporous Anodic Alumina Layers and Cell Adherence. *Acta Biomater.* **2014**, *10*, 968−974.
(22) Sayari, A.; Heydari-Gorji, A.; Yang, Y. CO_2-induced Degradation of Amine-Containing Adsorbents: Reaction Products and Pathways. *J. Am. Chem. Soc.* **2012**, *134*, 13834−13842.
(23) Zhou, Y.; Tao, Y. F.; Yang, J.; Lin, W. G.; Wan, M. M.; Wang, Y.; Zhu, J. H. Novel Phenol Capturer Derived from the As-Synthesized MCM-41. *J. Hazard. Mater.* **2011**, *190*, 87−93.
(24) Yeh, T. F.; Syu, J. M.; Cheng, C.; Chang, T. H.; Teng, H. Graphite Oxide as a Photocatalyst for Hydrogen Production from Water. *Adv. Funct. Mater.* **2010**, *20*, 2255−2262.
(25) Zhao, D. Y.; Feng, J. L.; Huo, Q. S.; Melosh, N.; Fredrickson, G. H.; Chmelka, B. F.; Stucky, G. D. Triblock Copolymer Syntheses of Mesoporous Silica with Periodic 50 to 300 Ångstrom Pores. *Science* **1998**, *279*, 548−552.
(26) Lin, H. P.; Wong, S. T.; Mou, C. Y.; Tang, C. Y. Extensive Void Defects in Mesoporous Aluminosilicate MCM-41. *J. Phys. Chem. B* **2000**, *104*, 8967−8975.
(27) (a) Wei, F.; Yang, J. Y.; Gao, L.; Gu, F. N.; Zhu, J. H. Capturing Nitrosamines in Tobacco-Extract Solution by Hydrophobic Mesoporous Silica. *J. Hazard. Mater.* **2009**, *172*, 1482−1490. (b) Jaroniec, M.; Solovyov, L. A. Improvement of the Kruk−Jaroniec−Sayari Method for Pore Size Analysis of Ordered Silicas with Cylindrical Mesopores. *Langmuir* **2006**, *22*, 6757−6760.
(28) Frisch, M. J.; Trucks, G. W.; Schlegel, H. B.; Scuseria, G. E.; Robb, M. A.; Cheeseman, J. R.; Zakrzewski, V. G.; Montgomery, J. A.; Stratmann, R. E.; Burant, J. C.; Dapprich, S.; Millam, J. M.; Daniels, A. D.; Kudin, K. N.; Strain, M. C.; Farkas, O.; Tomasi, J.; Barone, V.; Cossi, M.; Cammi, R.; Mennucci, B.; Pomelli, C.; Adamo, C.; Clifford, S.; Ochterski, J.; Petersson, G. A.; Ayala, P. Y.; Cui, Q.; Morokuma, K.; Malick, D. K.; Rabuck, A. D.; Raghavachari, K.; Foresman, J. B.; Cioslowski, J.; Ortiz, J. V.; Baboul, A. G.; Stefanov, B. B.; Liu, G.; Liashenko, A.; Piskorz, P.; Komaromi, I.; Gomperts, R.; Martin, R. L.; Fox, D. J.; Keith, T.; Al-Laham, M. A.; Peng, C. Y.; Nanayakkara, A.; Challacombe, M.; Gill, P. M. W.; Johnson, B.; Chen, W.; Wong, M. W.; Andres, J. L.; Gonzalez, C.; Head-Gordon, M.; Replogle, E. S.; Pople, J. A. *Gaussian 03*, Revision B. 01[CP]; Gaussian, Inc.: Pittsburgh, PA, 2003.
(29) Yue, M. B.; Chun, Y.; Cao, Y.; Dong, X.; Zhu, J. H. CO_2 Capture by As-Prepared SBA-15 with an Occluded Organic Template. *Adv. Funct. Mater.* **2006**, *16*, 1717−1722.
(30) Güllüoglu, M. T.; Erdogdu, Y.; Karpagamb, J.; Sundaraganesan, N.; Yurdakul, S. DFT, FT-Raman, FT-IR, and FT-NMR Studies of 4-Phenylimidazole. *J. Mol. Struct.* **2011**, *990*, 14−20.
(31) (a) Zhang, Z.; Pinnavaia, T. J. Mesostructured γ-Al_2O_3 with a Lathlike Framework Morphology. *J. Am. Chem. Soc.* **2002**, *124*, 12294−12301. (b) Zukal, A.; Siklová, H.; Cejka, J. Grafting of Alumina on SBA-15: Effect of Surface Roughness. *Langmuir* **2008**, *24*, 9837−9842.
(32) Wang, X. X.; Ma, X. L.; Song, C. S.; Locke, D. R.; Siefert, S.; Winans, R. E.; Möllmer, J.; Lange, M.; Möller, A.; Gläser, R. Molecular Basket Sorbents Polyethylenimine-SBA-15 for CO_2 Capture from Flue Gas: Characterization and Sorption Properties. *Microporous Mesoporous Mater.* **2013**, *169*, 103−111.
(33) Wang, J. L.; Cheng, F.; Zhu, P. X. Structure and Properties of Urea-Plasticized Starch Films with Different Urea Contents. *Carbohydr. Polym.* **2014**, *101*, 1109−1115.
(34) Prasanyaa, T.; Jayaramakrishnan, V.; Haris, M. Synthesis, Optical, Thermal and Second Harmonic Generation Studies of Pure, Urea and Thiourea Doped Organic L-Tartaric Acid-Nicotinamide (LTN) Crystals. *Optik (Munich, Ger.)* **2014**, *125*, 732−736.
(35) Goryashenko, S. S.; Park, Y. K.; Kim, D. S.; Park, S. E. Mechanistic Study of the SCR of NO with Propylene over Co/ZSM-5 Using In-Situ FT-IR. *Res. Chem. Intermed.* **1998**, *24*, 933−951.
(36) Ceraulo, L.; Dormond, E.; Mele, A.; Liveri, V. T. FT-IR and Nuclear Overhauser Enhancement Study of the State of Urea Confined in AOT-reversed Micelles. *Colloids Surf., A* **2003**, *218*, 255−264.
(37) Xavier, R. J.; Dinesh, P. Spectroscopic (FT-IR, FT-Raman, ^{13}C and ^{1}H NMR) Investigation, Molecular Electrostatic Potential, Polarizability, and First-Order Hyperpolarizability, FMO and NBO Analysis of 1-methyl-2-imidazolethiol. *Spectrochim. Acta, Part A* **2014**, *118*, 999−1011.
(38) (a) Huang, J. H.; Ruther, T. Why are Ionic Liquids Attractive for CO_2 Absorption? An Overview. *Aust. J. Chem.* **2009**, *62*, 298−308. (b) Nachtigall, P.; Grajciar, L.; Perez-Pariente, J.; Pinar, A. B.; Zukal, A.; Cejka, J. Control of CO_2 Adsorption Heats by the Al Distribution in FER Zeolites: Effect of Synthesis Conditions. *Phys. Chem. Chem. Phys.* **2012**, *14*, 1117−1120.
(39) Reitmeier, S. J.; Gobin, O. C.; Jentys, A.; Lercher, J. A. 41-Role of Transport Processes on the Shape Selective Properties of HZSM-5. *Angew. Chem., Int. Ed.* **2008**, *47*, 1−7.